Technical Physics, 2022, Vol. 67, No. 2

07

Degradation of InGaN/GaN quantum well UV LEDs caused by short-term exposure to current

©
A.M. Ivanov, A.V. Klochkov

Ioffe Institute,
194021 St. Petersburg, Russia
e-mail: alexandr.ivanov@mail.ioffe.ru

Received August 4, 2021
Revised November 16, 2021
Accepted November 16, 2021

A comparative analysis of the initial stages of degradation of ultraviolet and blue LED structures with InGaN/GaN quantum wells is carried out. In the mode of accelerated aging, the structures were subjected to short-term, sequential exposure to currents of 80−190 mA at forward bias. The exposure time did not exceed three hours. There was an increase (up to 20%) in the external quantum efficiency. The most probable physical mechanisms explaining the changes in InGaN/GaN LEDs are presented and possible ways to slow down the aging of UV LEDs are outlined.

Keywords: Degradation of ultraviolet light-emitting diodes, increase in quantum efficiency, slowing down the aging.

DOI: 10.21883/TP.2022.02.52953.229-21

Introduction

The wide use of semiconductor ultraviolet (UV) light-emitting diodes and lasers in various branches of the instrument-making industry for optoelectronics, biology, medicine and sanitation arouses keen interest among researchers in the morphology of InGaN- and AlGaN-nanostructure and physical processes taking place in contemporary instruments based on quantum wells and quantum dots.

Since UV light-emitting diodes have a smaller efficiency and a shorter service life as compared to visible range LEDs, the study of their degradation processes is an important task due to the expansion of application areas and an increased production of optoelectronic device of this radiation range, particularly in medicine where degradation of devices is undesirable (it is difficult for a medical worker to visually note changes in optical radiation in the UV range). This is confirmed by contemporary studies [1–6].

Consideration of the reasons for degradation of semiconductor nanostructures presupposes studying of the aspects of change in the main physical parameters of LEDs and lasers based on nitride materials: comparing the behavior of UV and visible region devices, and, in the first place, a drop in external quantum efficiency. Understanding of the composition and nature of occurring defects is required to improve the technology for manufacture of UV GaN-LED based on quantum wells in order to enhance their reliability and extend the service life. Despite the large number of papers, there is no unified idea of the nature of LED aging and failures.

Earlier papers explained the LED degradation mechanisms, in particular, under exposure to direct current, by an increase in contact resistance [7], migration of ions of gallium and indium metallic impurities across a system of extended defects simultaneously with inhomogeneous generation of defects [8], formation of tunnel conductive paths via activation of helical dislocations [9] and catastrophic failures due to macroscopic defects that can be avoided by optimizing the growth process [10]. The present-day ideas relate the degradation of UV LEDs and lasers to the formation of nonradiative recombination centers in active regions and barriers, as well as to changes with doping impurities in the *p*- and *n*-regions.

Structural solutions for the technological design of structures enable an improvement in the actual parameters of devices and facilitate an extension of their service life through hindering of degradation processes. The build-up of the active area of a *p*-contact hinders degradation due to the increase of current density, while an increase in the number of quantum wells adjusts the distribution of carriers in the active region and reduces the Auger recombination [11].

Electrons in nitride materials have a smaller effective mass as compared to holes and, accordingly, a higher mobility. They more easily pass through a sequence of quantum wells and barriers and accumulate in the last quantum well near a *p*-region. Movement of holes to a *n*-region is hindered. It was established (by calculation) that an increase of quantum well width and a decrease of barrier thickness reduces the potential barrier for holes and increases the barrier for electron leak, thus causing a rise in quantum efficiency [12]. Fluctuations of indium composition with increase of quantum well width enhance luminescence due to the growing localization potential [13]. It is reasonable to use additional layers [14–16], superlattices [17,18] and barriers of a special shape [19,20], which increase the overlap of the wave functions of the electron and hole in quantum wells and, consequently, the radiative recombination rates.

This is also facilitated by a decrease of the quantum-confined Stark effect [13] and polarization fields [12,21,22].

A peculiarity of many contemporary papers on structural improvement of LED structures with quantum wells is the theoretical nature. Improvement of device characteristics is presented on the basis of mathematical modeling.

The present paper is aimed at a comparative analysis of the initial stages of aging processes in UV and blue (described earlier in [23]) LEDs based on InGaN/GaN-quantum wells. The objects, as distinct from many research papers, were indicator LEDs manufactured by the proven large-scale industrial technology. The distinctive features of the study are the LED aging conditions: changes in LEDs took place at short-time (maximum three hours) successive exposures of specimens to a direct current of 80 to 190 mA at forward bias. The applied currents were many times higher than the LED operating currents and caused simultaneous heating of the structures under study. The operability of these devices under strong overloads as compared to the operating modes has been demonstrated. The maximum rise of external quantum efficiency at the initial stages of exposure to current was 20%. In subsequent tests by high currents, the positive phenomena gave place to degradation processes. Suggested mechanisms for an initial improvement of UV LEDs — characteristics were presented and possible technological methods (not related to structural changes) were outlined for delaying their aging.

1. Experiment description

Current-voltage characteristics and light characteristics of UV LEDs with InGaN/GaN-quantum wells were measured using a Keysight (Agilent) 34401A digital voltmeter and a GPS-4303 power source. Currents in current dependence measurements were set by means of resistance box R33. A specially developed capsule provided rigid binding (at a fixed distance) of the measured commercial indicator LEDs of the same geometry to a measuring photodiode. The used layout and sensitivity of devices allowed for measurement of nanoampere currents. Temperature of the LED housing was monitored using the NXFT15WF thermistor. The FD-24K silicon photodiode was used to measure only relative changes in radiation intensity and external quantum efficiency η.

The study was carried out using InGaN/Ga-LEDs manufactured by Betlux — BL-L522VC with peak radiation energy $h\nu_{QW} = 3.06$ eV or radiation wavelength $\lambda = 405$ nm and manufactured by Nichia — NSPU510CS, $h\nu_{QW} = 3.31$ eV, $\lambda = 375$ nm, $\eta \leq 30\%$, as well as NSPB300, $h\nu_{QW} = 2.67$ eV, $\lambda = 465$ nm, $\eta = 15\%$; the main results are presented in [23] with rated currents $J = 20$ mA and actual diode area $\sim 10^{-3}$ cm^2.

To analyze UV LED degradation processes, it was suggested to test the devices by short-time exposures with current passage (in the range $J = 80-190$ mA) at forward bias. The duration of each test was from 10 min to 3 h.

Table 1. Successive testing of LEDs X and Y at forward bias

Test №	Direct current J, mA	Power W, W	Time t, h	η/η_{init} at J=9 mA, %
LED X				
1	80	0.294	1.33	120
2	120	0.466	3	98
3	150	0.615	2	55
4	170	0.726	0.5	42
LED Y				
1	80	0.285	1.17	118
2	120	0.445	3	119
3	150	0.569	2	108
4	170	0.656	0.5	107
5	180	0.700	0.5	97
6	190	0.739	1.5	70

Changes in current-voltage and current dependences (optical power and external quantum efficiency) were studied after each successive stage of an electrical action on a LED.

The UV LEDs BL-L522VC, NSPU510CS and blue ones NSPB300 will be denoted as X, Y and Z respectively for convenience of material presentation and perception.

2. Experimental results

Fig. 1 shows the changes in external quantum efficiency as a result of accelerated degradation tests under exposure to current at forward bias for LEDs X and Y vs. quantity of electricity passing through the device.

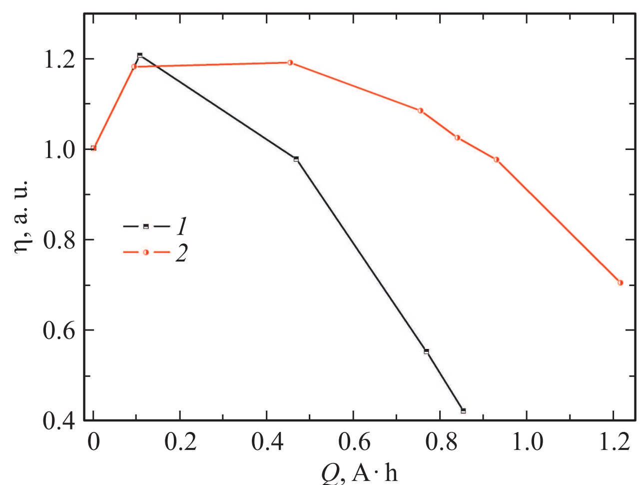

Figure 1. Plots of external quantum efficiency vs. quantity of electricity passing through the LEDs: *1, 2* — LEDs X, Y respectively.

Table 2. Successive testing of LEDs Z at forward bias

Test №	Direct current J, mA	Power W, W	ΔT, °C	Time t, h	η/η_{init} at $J = 20$ mA, %
LED Z					
1	150	0.585	105	1	92
2	150	0.585	105	1	120
3	150	0.585	105	0.5	121

Note. ΔT is the minimum overheat of the active region.

After test №1 (80 mA, $\sim$ 1 h) there is a rapid increase of quantum efficiency of LEDs X and Y, which is $\sim$ 20%, and insignificant changes after test №2 (120 mA/(3 h), diode Y). Subsequent decrease of quantum efficiency is most abrupt during tests №3 — 150 mA/(2 h) and №4 — 170 mA/(0.5 h) for LED X, and for LED Y — during tests №5 — 180 mA/(0.5 h), №6 — 190 mA/(1.5 h). A drop in quantum efficiency in LEDs X is observed under exposure to smaller currents than in LEDs Y. The data on the UV LEDs is given in Table 1 (η_{init} is external quantum efficiency of the initial specimen). The behavior of the UV LEDs differs from LEDs Z, first of all, by the brevity of observed changes: after the first exposure to 150 mA/(1 h) (150 A/cm^2, 1 h) the efficiency of Z did not change, after the second exposure to 150 mA/(1 h) it dropped by 18%, and after the third exposure to 150 mA/(0.5 h) the external quantum efficiency increased by 14% as compared to the initial value. The preliminary exposures to currents of 80–120 mA did not change the efficiency. The required value for manifestation of changes in external quantum efficiency was $Q = 0.75\,\text{A}\cdot\text{h}$. Table 2 gives another aging conditions for diode Z.

Fig 2 shows the plots of radiation intensity (photoinduced current J_{ph}) vs. current through LED Y before and after

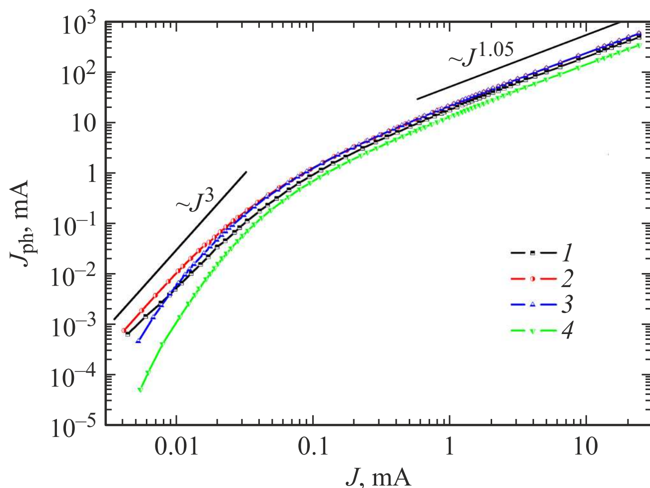

Figure 2. Plot of photoinduced current vs. current at forward bias of LED Y before (*1*) and three exposures to current (*2–4*): *2* — 80 mA/(1.17 h), *3* — 120 mA/(3 h), *4* — 190 mA/(1.5 h).

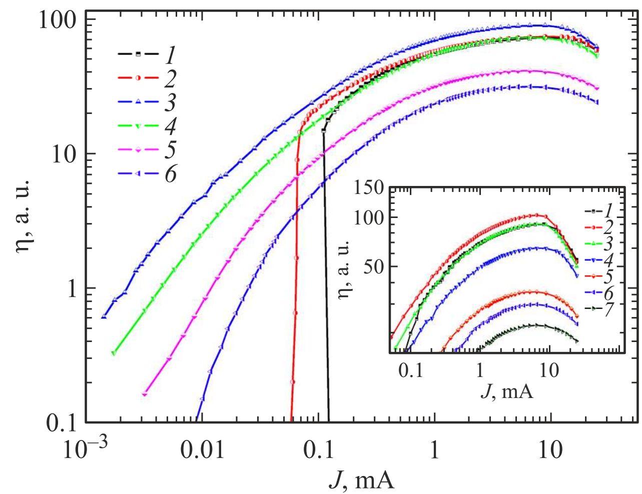

Figure 3. Plots of external quantum efficiency vs. current at forward bias of LED X before (*1, 2*) and after four successive exposures to current (*3–6*): *3* — 80 mA/(1.33 h), *4* — 120 mA/(3 h), *5* — 150 mA/(2 h), *6* — 170 mA/(0.5 h). In the insert — before (*1*) and after six successive exposures to current (*2–7*): *2* — 80 mA/(1.17 h), *3* — 105 mA/(3 h), *4* — 120 mA/(3 h), *5* — 150 mA/(2.5 h), *6* — 160 mA/(0.5 h), *7* — 170 mA/(0.5 h).

tests №1, 2, 6. The most significant differences in the plots occur at $J < 50\,\mu$A with an abrupt rise of $J_{ph} \propto J^3$. Optical power at these currents after test №2 is lesser than after test №1, while at $J < 7\,\mu$A it is lesser than the initial one. On the initial area of the plot, the drop of radiation intensity after test №6 is the highest (it differs from the initial plot by an order).

Fig 3 shows the current plots of external quantum efficiency before after tests №1–4 of diode X. The initial specimen in two successive measurements has a higher threshold current J_{th} that corresponds to the onset of LED radiation. The initial specimen has a lower efficiency at $J < 100\,\mu$A as compared to the specimens exposed to electric stresses by currents at forward bias, which is typical for specimens X, Y (Fig. 3, the insert) and is not related to leaks between contacts. Efficiency drop as compared to the initial value after tests №2–4 occurs not in the whole current range. The plots of efficiency vs. current are characterized by a mild maximum at $J = 9$ mA and a sloping drop of efficiency at high currents as distinct from diode Y, where a plateau was observed at medium and rated currents.

Fig. 4 shows the plots of current vs. voltage before and after tests №1–4 of diode X. The initial dependencies changed at two successive measurements. They had a sloping part at $U = 2.5$ V, which it not typical for InGaN-LEDs in measurements at forward bias. Current changed significantly after each test at low voltages, but the differences in current vs. voltage plots at medium and high voltages are insignificant. In order to determine ideality factor $n_J(U_J)$, current vs. voltage at a p–n-transition $J(U_J)$ was plotted on the basis of current-voltage characteristics

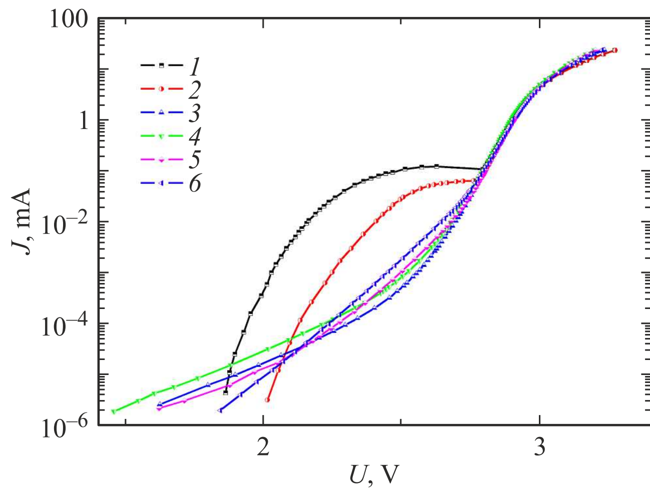

Figure 4. Plots of current vs. voltage $J(U)$ of LED X before (*1, 2*) and after four successive exposures to currents (*3–6*): *3* — 80 mA/(1.33 h), *4* — 120 mA/(3 h), *5* — 150 mA/(2 h), *6* — 170 mA/(0.5 h).

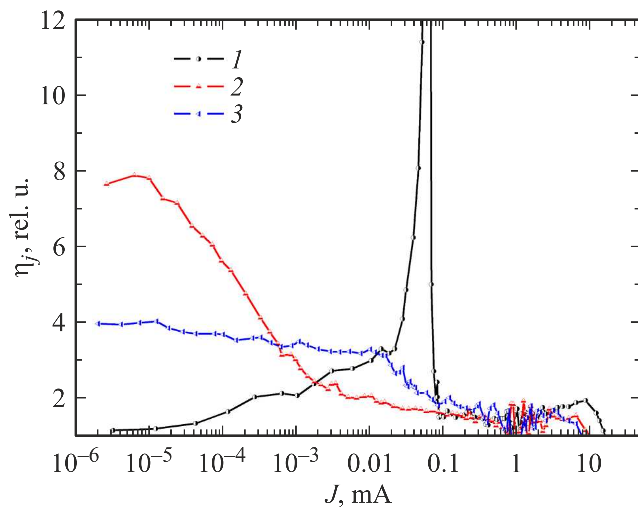

Figure 5. Plots of the ideality factor vs. current of LED X before (*1*) and after two exposures to current (*2, 3*): *2* — 80 mA/(1.33 h), *3* — 170 mA/(0.5 h).

(Fig. 4). Series resistance r_s was determined from the linear region $J(U)$ of the characteristic; it was $10.8\,\Omega$, $U_J = U - Jr_s$. The plots of $J(U_J)$ are approximated by exponential function $J(U_J) \propto \exp(qU_J/n_J(U_J)kT)$, q is the elementary charge, kT is thermal power. They were used to calculate dependencies $n_J(J) = (q/kT)/(\mathrm{d}\ln J/\mathrm{d}U_J)$.

Fig. 5 shows the curves of the ideality factor vs. current $n_J(J)$ before and after tests №1, 4 of diode X. The initial specimen had an anomalous rise of n_J related to a ledge on the current vs. voltage plot. The magnitude of $n_J(J)$ was ≥ 3 for $J < 1\,\mu$A in the specimen exposed to successive current stresses. A drop in $n_J(J) \leq 2$ is observed in the operating current region on all the plots.

3. Discussion of results

Manufacturers state a long service life of semiconductor LEDs — tens of thousands of hours. This data is obtained by extrapolating the results of observation of LED aging in extreme conditions (increased current and temperature of the crystal). CREE Company, for instance, uses the JESD22 standard: the maximum permissible current for 1008 h. According to JESD22, a 15% decrease of luminous flux means a device malfunction. Non-standard behavior of LEDs, e.g. a rise in optical radiation at the initial aging stage, as our studied have demonstrated, can affect the accuracy of service life estimation.

Fig. 1 and Table 1 shows a rise in external quantum efficiency of UV LEDs $\sim 20\%$ after tests №1 and its subsequent drop after tests №3–6. A comparison of our results with the studies of long-term LED degradation reveals two peculiarities of the observed results:

a) the experiments do not show a rise in optical power of radiation under aging by increased currents [24,25];

b) a rise is observed but is rather insignificant as compared to the rise we observed — at the level of several percent $\leq 5\%$ (5% only in a part of the studied LEDs [8]) and the authors either do not draw readers' attention to it [7,26] (in our opinion, they might consider it as a measurement error [27]) or, as distinct from our current vs. voltage plots, a rise is accompanied by a voltage increase due to degradation of the ohmic contact [7,28].

Different mechanisms manifest themselves in the degradation of UV and blue LEDs based on InGaN/GaN-quantum wells. Hydrogen can form an electrically neutral Mg–H complex and accumulate together with H^+ in p-layers and in the active region. Mg–H breaks down due to an impact of hot carriers, Joule heating and reverse absorption of radiation. H migrate by diffusion and drift in an electric field towards the n-side. The following takes place due to the in-service accumulation of acceptor defects near or in the active region: n-doping is partially compensated, nonradiative recombination centers originate, stray current might occur [1,2].

Positive changes are possible at the initial stages — rise of optical power, decrease of operating voltage, observed not in all LED aging experiments. This is related to the competition of processes that change the rates of radiative and nonradiative recombination. A rise in the carrier concentration (activation of Mg, disintegration of Mg–H defect, a rise in hole concentration, for more detail see [23]) enhances the radiative recombination. Defect formation takes place at the same time. Defect formation, movement and annealing can take place due to the energy released near a defect during recombination (the energy is close to the band gap) [29]. Each Shockley–Read–Read recombination event and Auger recombination event liberates sufficient energy for the breaking of defect–impurity bonds in GaN, thus facilitating the defect generation in quantum wells [24].

A concentration rise is mainly noted for point defects involved in nonradiative SRH-recombination; in the tunnel

transport of carriers into quantum wells. The deep-level spectrum in the band gap of InGaN/GaN-quantum structures changes under a stress impact. An increase in the share of deeper centers increases the efficiency drop [25,30]. By contract, the formation of smaller transport levels, which ensure tunneling on defects, facilitates its rise [31], since it helps the carriers overcome the potential barriers. These processes result in a rise of radiation intensity after tests №1,2 (Fig. 2) in our study. Severe testing by high currents causes a local heating of defects by phonons, which leads to a change in nonradiative recombination rate [29]. The decisive process is the origination of deeper centers accountable for nonradiative recombination: LED efficiency decreases (Fig. 1, 3).

Total current to a quantum well is divided into the current that defines radiative recombination and the current associated with nonradiative recombination and losses. A universal provision in the consideration of recombination processes in InGaN/GaN-quantum wells is the ABC model (e.g., [32]) for internal quantum efficiency:

$$\eta_{\text{int}} = \frac{Bn^2}{An + Bn^2 + Cn^3},$$

where n is carrier concentration, A, B, C are coefficients of nonradiative, radiative and Auger recombination. According to [33,34], the denominator must include summand $f(n)$, related to the current of charge carrier leakage from quantum wells. When the injection level is high, polarization fields and an increasing defect rate of barriers that adjoin the active regions cause an outflow of carriers from quantum wells [35]. Auger recombination becomes the predominant recombination mechanism [32]. Auger recombination under the current stress impact of 80 A/cm^2 (it corresponds to the current density of test №1 in our study) is 66% of the total recombination, while SRH is only 1.4% [24].

Two recombination components are usually considered in case of low injection levels [36]:

$$\frac{I}{q}\eta_i = V(An + Bn^2),$$

where I is current density, η_i is carrier injection efficiency, V — active region volume. $A \propto N\sigma v_{th}$, i.e. proportional to defect density, carrier capture cross-section, thermal velocity,on the assumption of their equality for both carrier types [37]. In accelerated aging conditions, quantity A, related to the nonradiative recombination rate, is not permanent but depends on changes in the defect spectrum. A rise in defect concentration (particularly those with the deepest levels) and a possible increase in carrier capture cross-sections increase quantity A and are the main mechanisms of UV LED degradation.

Plot $J_{ph} \propto J^3$ in Fig. 2 becomes smoother as current increases — $J_{ph} \propto J^{1.05}$. The inflection point approximately corresponds to the point of transition to a smoother plot of current vs. radiative recombination rate in the calculations according to the ABC-model [24]. Efficiency in the low current range is limited by SRH-losses.

Fig. 3 shows that J_{th} increases in successive tests №2−4. The increase in threshold current J_{th} is due to the motion of point defects towards the active region [38]. $J_{th} \propto n_{th}/\tau$, n_{th} is carrier threshold density, τ is recombination lifetime. The latter is determined by recombination coefficients A, B, C. An increase of J_{th} correlates with an increase of quantity A, and no changes in B and C are anticipated after current stresses [39]. In the initial specimen before the exposure, we have $J_{th} \sim 100\,\mu$A and it decreases by two orders ($J_{th} \sim 1\,\mu$A) after the exposure to current (test №1, 80 mA, ~ 1 h), accompanied with a rise in external quantum efficiency. The corresponding changes in the defect spectrum entail a drop in quantity A and the nonradiative recombination rate.

Several areas having different slopes can be distinguished in Fig. 4 of the current vs. voltage plot for diode X. With $U \leq 2.8$ V the current noticeably changes after tests №1−4. Diodes X do not display a monotonous shift of the plots towards the region of lower voltages as in diodes Y. Current increase under a constant bias is explained by changes in the defect spectrum and increase of the levels involved in tunneling of carriers (trap-assisted tunneling (TAT), hopping) to the active region [3,5,38,40,41]. The plots under exposures to the currents of 150 and 170 mA shift towards the region of higher voltages. The presence of flat plot areas at $U \approx 2.5$ V for the initial specimen manifests itself in an abnormal rise of the ideality factor magnitude (Fig. 5).

Steepness of the current plot increases on the intermediate area at $2.9 \geq U \geq 2.8$ V, which can be due to a rise of injection and tunnel transparency of barriers. $n_J(J) \leq 2$, while efficiency increase slows down (Fig. 3). Changes $J(U)$ do not occur after the exposures to current.

Injection current prevails on the area of currents $J \geq 1.0$ mA. Efficiency reaches the maximum and starts slowly decreasing, which corresponds to intensification of nonradiative recombination; $n_J(J)$ tends to unity.

It can be seen in Fig. 5 that quantity $n_J(J) \geq 3$ at currents $J < 1\,\mu$A after tests №1, 4. Such large magnitudes of the ideality factor correspond to the presence of defect-assisted carrier hopping [42]. The noted increase in quantity $n_J(J)$ as compared to the initial specimen due to the current stresses indicates a rise in the concentration of deep levels, which facilitate the overcoming of potential barriers by the carriers on the basis of trap-assisted conductivity [25].

The recorded effects of an increase of optical power, external quantum efficiency under current stress actions at forward bias, accompanied by Joule heating ($\Delta T \sim 100^\circ$C [23]), in industrial InGaN-LEDs indicate, in the authors' opinion, a possible improvement of their initial characteristics during manufacture (e.g., by a higher activation of Mg). Diodes X, Y and Z demonstrate different „resistance" to exposure to current, since their efficiency drops at different exceeded values of the nominal current (20 mA).

The previously observed increase of quantum efficiency under long-term exposures to current [43] presupposes two directions for service life extension and improvement of

characteristics of InGaN- and AlGaN-optoelectronic device with quantum wells. The structural solutions described in the overview are based mainly on the peculiarities of growth and combination of epitaxial layers.

Another way to enhance efficiency and hinder degradation is increase of injection. The main doping element for a p-region is Mg. A growing concentration of holes in a p-region can be possibly attained by increasing the concentration of Mg, increasing its activation by electric current [5], breakdown of the Mg−H defect, growth of p-layers not in a hydrogen stream but in a nitrogen stream. The latter requires additional studies since degradation of external quantum efficiency and generation-recombination noise in the studied UV LEDs are related to an electron trap E_c — 0.8 eV [44]. Defects located in InGaN/GaN-quantum wells are due to interstitial nitrogen, and a rise in its concentration can accelerate UV LED degradation. Origination of nonradiative defects in [24] can be also due to nitrogen.

Increase of Mg doping is limited by self-compensation of the Mg impurity [45,46]; by formation of Mg-based donor-type defects (Mg_i-V_N, $Mg_{Ga}-V_N$). Selection of the optimal doping conditions and annealing conditions is important for synthesis of epitaxial p-GaN layers having a low resistance [47].

4. Findings

1) A comparison of degradation processes in blue LEDs (Fig. 1, Table 1, 2) has shown that initial changes in blue LEDs require higher currents as compared to the rated ones than those for UV LEDs. Thereat, the maximum rise of η for the considered UV and blue LEDs was $\sim 20\%$. From the two UV LED types, degradation begins sooner in LEDs X. The differences in the behavior of LEDs Z and UV LEDs X, Y are probably due to the different band gap and, accordingly, energy liberated in nonradiative recombination. This gives rise to differences in defect spectrum changes, namely, its changes define the LED aging processes.

2) The observed increase of external quantum efficiency must be taken into account by device developers when estimating the LED service life. Additional studies of long-term degradation may show whether the LED service life increases after a short-term current stress action accompanied by a rise in external quantum efficiency.

Conclusion

The performed comparative analysis of commercial indicator UV and blue LEDs using a set of ultra-short (≤ 3 h), sequential exposures to currents (in a wide range of 80−190 mA) at forward bias has demonstrated the possibility of an improvement in their characteristics. Changes in UV LEDs begin at smaller current loads as compared to blue LEDs. The suggested exposure method allowed for observing a rise in radiation intensity and external quantum efficiency (up to 20%) in UV and blue LEDs, which was not related to long-term processes. Changes in the defect spectrum with an increase in the levels that provide tunneling on defects determine the conductivity improvement during carrier motion to a quantum well. Subsequent exposures to high currents led to a rise in the concentration of SRH-centers and a drop in quantum efficiency. The authors believe that slowing down of aging and improvement of characteristics in LED structures with quantum wells based on nitride materials can be attained through better activation of Mg and action on the defect spectrum in order to improve the carrier transport. The possibility to grow p-layers in a nitrogen stream, and not in a hydrogen stream, for the same purpose required additional studies.

Conflict of interest

The authors declare that they have no conflict of interest.

References

[1] J. Glaab, J. Haefke, J. Ruschel, M. Brendel, J. Rass, T. Kolbe, A. Knauer, M. Weyers, S. Einfeldt, M. Guttmann, C. Kuhn, J. Enslin, T. Wernicke, M. Kneissl. J. Appl. Phys., **123**, 104502 (2018). DOI: 10.1063/1.5012608

[2] J. Glaab, J. Ruschel, T. Kolbe, A. Knauer, J. Rass, H.K. Cho, N. Lobo Ploch, S. Kreutzmann, S. Einfeldt, M. Weyers, M. Kneissl. IEEE Photonics Technol. Lett., **31** (7), 529 (2019). DOI: 10.1109/LPT.2019.2900156

[3] H. Xiu, Y. Zhang, J. Fu, Z. Ma, L. Zhao, J. Feng. Curr. Appl. Phys., **19**, 20 (2019). DOI: 10.1016/j.cap.2018.10.019

[4] Z. Ma, A. Almalki, X. Yang, X. Wu, X. Xi, J. Li, S. Lin, X. Li, S. Alotaibi, M. Al huwayz, M. Henini, L. Zhao. J. Alloys Compd., 845, 156177 (2020). DOI: 10.1016/j.jallcom.2020.156177

[5] Z. Ma, H. Cao, S. Lin, X. Li, L. Zhao. Solid State Electron., **156**, 92 (2019). DOI: 10.1016/j.sse.2019.01.004

[6] D. Monti, M. Meneghini, C. De Santi, G. Meneghesso, E. Zanoni., J. Glaab, J. Rass, S. Einfeldt, F. Mehnke, J. Enslin, T. Wernicke, M. Kneissl. IEEE Trans. Electron Devices, **64** (1), 200 (2017). DOI: 10.1109/TED.2016.2631720

[7] M. Meneghini, D. Barbisan, Y. Bilenko, M. Shatalov, J. Yang, R. Gaska, G. Meneghesso, E. Zanoni. Microelectron. Reliab., **50**, 1538 (2010). DOI: 10.1016/j.microrel.2010.07.089

[8] A.L. Zakheim, M.E. Levinshtein, V.P. Petrov, A.E. Chernyakov, E.I. Shabunina, N.M. Shmidt. Semicond., **46** (2), 208 (2012). DOI: 10.1134/S106378261202025X

[9] A. Pinos, S. Marcinkevičius, M.S. Shur. J. Appl. Phys., **109**, 103108 (2011). DOI: 10.1063/1.3590149

[10] Z. Gong, M. Gaevski, V. Adivarahan, W. Sun, M. Shatalov, M. Asif Khan. Appl. Phys. Lett., **88**, 121106 (2006). DOI: 10.1063/1.2187429

[11] J. Ruschel, J. Glaab, B. Beidoun, N.L. Ploch, J. Rass, T. Kolbe, A. Knauer, M. Weyers, S. Einfeldt, M. Kneissl. Photonics Res., **7** (7), B36 (2019). DOI: 10.1364/PRJ.7.000B36

[12] H. Dong, T. Jia, J. Liang, A. Zhang, Z. Jia, W. Jia, X. Liu, G. Li, Y. Wu, B. Xu. Opt. Laser Technol., **129**, 106309 (2020). DOI: 10.1016/j.optlastec.2020.106309

[13] J. Huang, W. Liu, L. Yi, M. Zhou, D. Zhao, D. Jiang. Superlattices Microstruct., **113**, 534 (2018). DOI: 10.1016/j.spmi.2017.11.036
[14] L. Wang, W. He, T. Zheng, Z. Chen, S. Zheng. Superlattices Microstruct., **133**, 106188 (2019). DOI: 10.1016/j.spmi.2019.106188
[15] M.R. Kwon, T.H. Park, T.H. Lee, B.R. Lee, T.G. Kim. Superlattices Microstruct., **116**, 215 (2018). DOI: 10.1016/j.spmi.2018.02.033
[16] N. Liu, H. Gu, Y. Wei, S. Zheng. Superlattices Microstruct., **141**, 106492 (2020). https://doi.org/10.1016/j.spmi.2020.106492
[17] X. Wang, H.-Q. Sun, Z.-Y. Guo. Opt. Mater., **86**, 133 (2018). DOI: 10.1016/j.optmat.2018.09.037
[18] R.K. Mondal, V. Chatterjee, S. Pal. Opt. Mater., **104**, 109846 (2020). DOI: /10.1016/j.optmat.2020.109846
[19] W. Guo, F. Xu, Y. Sun, L. Lu, Z. Qin, T. Yu, X. Wang, B. Shen. Superlattices Microstruct., **100**, 941 (2016). http://dx.doi.org/10.1016/j.spmi.2016.10.070
[20] Q. Wang, L. He, L. Wang, C. Li, C. He, D. Xiong, D. Lin, J. Wang, N. Liu, Z. Chen, M. He. Opt. Commun., **478**, 126380 (2021). DOI: 10.1016/j.optcom.2020.126380
[21] Y. Zhang, L. Yu, K. Li, H. Pi, J. Diao, X. Wang, Y. Shen, C. Zhang, W. Hu, W. Song, S. Li. Superlattices Microstruct., **82**, 151 (2015). DOI: 10.1016/j.spmi.2015.02.004
[22] L. Wang, G. Li, W. Song, H. Wang, X. Luo, Y. Sun, B. Zhang, J. Jiang, S. Li. Superlattices Microstruct., **122**, 608 (2018). DOI: 10.1016/j.spmi.2018.06.039
[23] A.M. Ivanov. Tech. Phys., **66** (1), 71 (2021). DOI: 10.1134/S1063784221010114
[24] N. Renso, C. De Santi, A. Caria, F. Dalla Torre, L. Zecchin, G. Meneghesso, E. Zanoni, M. Meneghini. J. Appl. Phys., **127**, 185701 (2020). DOI: 10.1063/1.5135633
[25] F. Piva, C. De Santi, M. Deki, M. Kushimoto, H. Amano, H. Tomozawa, N. Shibata, G. Meneghesso, E. Zanoni, M. Meneghini. Microelectron. Reliab., **100**–**101**, 113418 (2019). DOI: 10.1016/j.microrel.2019.113418
[26] T. Yu, S. Shang, Z. Chen, Z. Qin, L. Lin, Z. Yang, G. Zhang. J. Lumin., **122**–**123**, 696 (2007). DOI: 10.1016/j.jlumin.2006.01.263
[27] M. Buffolo, C. De Santi, M. Meneghini, D. Rigon, G. Meneghesso, E. Zanoni. Microelectron. Reliab., **55**, 1754 (2015). http://dx.doi.org/10.1016/j.microrel.2015.06.098
[28] J. Fu, L. Zhao, H. Cao, X. Sun, B. Sun, J. Wang, J. Li. AIP Adv. **6**, 055219 (2016). http://dx.doi.org/10.1063/1.4953056
[29] I.N. Yassievich. Semicond. Sci. Technol. **9**, 1433 (1994).
[30] M. La Grassa, M. Meneghini, C. De Santi, E. Zanoni, G. Meneghesso. Microelectron. Reliab., **64**, 614 (2016). DOI: 10.1016/j.microrel.2016.07.131
[31] N.I. Bochkareva, A.M. Ivanov, A.V. Klochkov, V.A. Tarala, Y.G. Shreter. Tech. Phys. Lett., **42** (11), 1099 (2016). DOI: 10.1134/S1063785016110146
[32] S.Yu. Karpov. Opt. Quantum Electron. **47**, 1293 (2015). DOI: 10.1007/s11082-014-0042-9
[33] Q. Lv, J. Gao, X. Tao, J. Zhang, C. Mo, X. Wang, C. Zheng, J. Liu. J. Lumin., **222**, 117186 (2020). DOI: 10.1016/j.jlumin.2020.117186
[34] P. Sahare, B.K. Sahoo. Mater. Today: Proceedings, **28**, 74 (2020). DOI: 10.1016/j.matpr.2020.01.303
[35] N. Trivellin, D. Montia, C. De Santia, M. Buffoloa, G. Meneghessoa, E. Zanonia, M. Meneghinia. Microelectron. Reliab., **88**–**90**, 868 (2018). DOI: 10.1016/j.microrel.2018.07.145
[36] M. Meneghini, N. Trivellin, K. Orita, S. Takigawa, M. Yuri, T. Tanaka, D. Ueda, E. Zanoni, G. Meneghesso. IEEE Electron Device Lett., **30** (4), 356 (2009). DOI: 10.1109/LED.2009.2014570
[37] J. Hu, L. Yang, M.W. Shin. J. Phys. D: Appl. Phys., **41**, 035107 (2008). http://dx.doi.org/10.1088/0022-3727/41/3/035107
[38] D. Monti, M. Meneghini, C. De Santi, G. Meneghesso, E. Zanoni, A. Bojarska, P. Perlin. Microelectron. Reliab., **76**–**77**, 584 (2017). DOI: 10.1016/j.microrel.2017.06.043
[39] M. Meneghini, G. Meneghesso, N. Trivellin, E. Zanoni, K. Orita, M. Yuri, D. Ueda. IEEE Electron Device Lett., **29** (6), 578 (2008). DOI: 10.1109/LED.2008.921098
[40] N.I. Bochkareva, Y.G. Shreter. Semicond., **52** (7), 934 (2018). DOI: 10.1134/S1063782618070035
[41] N.I. Bochkareva, A.M. Ivanov, A.V. Klochkov, Y.G. Shreter. J. Phys.: Conf. Ser., **1697**, 012203 (2020). DOI: 10.1088/1742-6596/1697/1/012203
[42] D. Zhu, J. Xu, A. Noemaun, J. Kim, E. Schubert, M. Crawford, D. Koleske. Appl. Phys. Lett., **94**, 081113 (2009). DOI: 10.1063/1.3089687
[43] M. Osinski, D.L. Barton. In coll.: *Introduction to Nitride Semiconductor Blue Lasers and Light Emitting Diodes,* ed. by S. Nakamura, S.F. Chichibu. (CRC Press, 2000), p. 386. ISBN 9780748408368
[44] I-H. Lee, A.Y. Polyakov, S-M. Hwang, N.M. Shmidt, E.I. Shabunina, N.A. Tal'nishnih, N.B. Smirnov, I.V. Shchemerov, R.A. Zinovyev, S.A. Tarelkin, S.J. Pearton. Appl. Phys. Lett., **111**, 062103 (2017). http://dx.doi.org/10.1063/1.4985190
[45] H.R. Qi, S. Zhang, S.T. Liu, F. Liang, L.K. Yi, J.L. Huang, M. Zhou, Z.W. He, D.G. Zhao, D.S. Jiang. Superlattices Microstruct., **133**, 106177 (2019). DOI: 10.1016/j.spmi.2019.106177
[46] Q. Xu, S. Zhang, B. Liu, T. Tao, Z. Xie, X. Xiu, D. Chen, P. Chen, P. Ha, Y. Zheng, R. Zhang. Superlattices Microstruct., **119**, 150 (2018). DOI: 10.1016/j.spmi.2018.04.053
[47] A.V. Mazalov, D.R. Sabitov, V.A. Kureshov, A.A. Padalitsa, A.A. Marmalyuk, R.Kh. Akchurin. Mod. Electron. Mater., **2**, 45 (2016). http://dx.doi.org/10.1016/j.moem.2016.09.003